Research Square

Preprints are preliminary reports that have not undergone peer review.
They should not be considered conclusive, used to inform clinical practice,
or referenced by the media as validated information.

Visible-light-driven degradation of tetracycline hydrochloride over 15 wt% Cu-doped CeO2 photocatalyst: Mechanism and performance study

Chengcheng Li

2249199305@qq.com

Independent Researcher

Research Article

Keywords: CeO_2, Cu loading, tetracycline hydrochloride, photocatalyst, charge separation

Posted Date: April 22nd, 2026

DOI: https://doi.org/10.21203/rs.3.rs-9477633/v1

License: This work is licensed under a Creative Commons Attribution 4.0 International License. Read Full License

Additional Declarations: The authors declare no competing interests.

Cu-Loaded CeO_2 Photocatalysts for Efficient Visible-Light Degradation of Tetracycline Hydrochloride

Abstract

In this study, a series of Cu nanoparticle-loaded CeO_2 (Cu-CeO_2) photocatalysts were successfully prepared through a hydrothermal route. The products were applied in the photocatalytic degradation of tetracycline hydrochloride (TCH) under visible light irradiation. The results showed that the 15 wt% Cu-CeO_2 sample achieved the best activity, degrading 85.3% of TCH within 60 min. The apparent reaction rate constant reached 33.84×10^{-3} min^{-1}, which was 5.12 times higher than that of pure CeO_2. The improved performance is mainly attributed to the narrowed bandgap, enhanced visible-light absorption, and accelerated charge separation efficiency induced by Cu loading. Based on characterization results and quenching experiments, a reasonable photocatalytic mechanism for TCH degradation over Cu-CeO_2 was proposed.

Keywords: CeO_2; Cu loading; tetracycline hydrochloride; photocatalyst; charge separation

1 Introduction

CeO_2 has attracted extensive attention in semiconductor photocatalysis due to its low toxicity, low cost, and high chemical stability. However, the practical application of pure CeO_2 is limited by its wide bandgap and fast recombination of photogenerated electron-hole pairs. Loading noble metal cocatalysts is a common strategy to enhance photocatalytic performance. For example, Keshvadi et al. prepared Ag-modified CeO_2 via wet impregnation, and the composite exhibited improved activity for methylene blue degradation. Huang et al. synthesized Au-loaded CeO_2 nanorods, which showed excellent performance in tetracycline degradation under visible light.

Nevertheless, the high cost and scarcity of noble metals restrict their large-scale application. Therefore, developing low-cost and high-performance CeO_2-based photocatalysts without noble metals is highly important for wastewater treatment. Copper is considered an ideal alternative cocatalyst owing to its low price, non-toxicity, and excellent electronic structure. In previous work, our group prepared Cu-modified Bi_2O_2S nanoflowers with enhanced TCH degradation efficiency. These results confirm that Cu modification can effectively boost the photocatalytic activity of CeO_2 for antibiotic removal.

In this work, Cu-loaded CeO_2 photocatalysts were synthesized via a simple hydrothermal method. The introduction of Cu nanoparticles significantly improved light absorption and charge separation efficiency. The optimized 15 wt% Cu-CeO_2 sample showed greatly enhanced activity

for TCH degradation compared with pure CeO_2. Combined with structural characterizations and mechanism tests, the photocatalytic degradation pathway was systematically analyzed.

2 Experimental

2.1 Synthesis of Cu-Loaded CeO_2 Photocatalysts

Pure CeO_2 was first prepared by a hydrothermal method according to previous reports. In a typical preparation of Cu-CeO_2, 100 mg of CeO_2 and a certain amount of $CuSO_4 \cdot 5H_2O$ were dissolved in 10 mL deionized water and stirred for 30 min. Then 600 μL of 1 M NaOH solution was added, followed by stirring for another 30 min. After that, 500 μL of 1 M $NaBH_4$ solution was added dropwise, and the mixture was stirred for 1 h. The precipitate was collected, washed with deionized water, and dried at 60 °C overnight to obtain 5 wt%, 15 wt%, and 20 wt% Cu-CeO_2 samples.

2.3 Characterization

X-ray diffraction (XRD) was carried out on a Rigaku Miniflex 600 diffractometer. X-ray photoelectron spectroscopy (XPS) was tested on a Thermo Fisher ESCALab 250Xi spectrometer. Scanning electron microscopy (SEM, ZEISS Crossbeam 540) was used to observe morphology and elemental distribution. UV-Vis diffuse reflectance spectra (DRS) were recorded on an Agilent Cary 100 spectrophotometer.

2.4 Photocatalytic Degradation Experiments

In a typical test, 20 mg of photocatalyst was dispersed in 40 mL of 50 mg/L TCH solution. The suspension was stirred in the dark for 30 min to reach adsorption-desorption equilibrium. A 150 W Xe lamp was used as the light source. At given intervals, 3.5 mL of solution was taken out and filtered. The concentration of TCH was measured at 375 nm using a UV-Vis spectrophotometer. All experiments were repeated twice.

3 Results and Discussion

The XRD patterns show that all samples present typical diffraction peaks of CeO_2 with cubic fluorite structure. No obvious Cu peaks are observed in 5 wt% Cu-CeO_2, indicating high dispersion of Cu nanoparticles. As Cu loading increases, characteristic peaks of Cu appear gradually.

UV-Vis spectra indicate that 15 wt% Cu-CeO_2 shows enhanced visible-light absorption due to the surface plasmon resonance effect of Cu. The bandgap of pure CeO_2 is 3.10 eV, while that of 15 wt% Cu-CeO_2 decreases to 2.74 eV, which favors light harvesting.

SEM images display that CeO_2 exhibits a nanorod morphology about 200 nm in length. Cu nanoparticles are uniformly distributed on the surface without destroying the original structure. EDX elemental mapping confirms the homogeneous distribution of Cu, Ce, and O.

XPS results verify the successful loading of Cu species. The Ce 3d spectra reveal the coexistence of Ce^{3+} and Ce^{4+}, and the ratio of Ce^{3+} increases after Cu modification. The O 1s spectra show lattice oxygen and adsorbed oxygen. The Cu 2p spectra prove the coexistence of Cu^{0} and Cu^{2+} due to partial oxidation during synthesis.

Photocatalytic tests show that pure CeO_2 has a low TCH degradation efficiency of only 34.1%. After Cu loading, the activity is greatly improved. The 15 wt% Cu-CeO_2 sample shows the highest efficiency of 85.3%. Further increasing Cu content to 20 wt% causes a decline in activity because of Cu nanoparticle aggregation.

The degradation efficiency is affected by pH value. Strong acidity and alkalinity both inhibit activity. Inorganic ions such as SO_4^{2-}, Ca^{2+}, and Mn^{2+} show obvious inhibitory effects. Cycling tests demonstrate that the catalyst remains stable after three runs.

PL spectra indicate that Cu-CeO_2 has lower fluorescence intensity than CeO_2, confirming suppressed carrier recombination. Quenching experiments prove that $\bullet O_2^-$ is the main active species during TCH degradation.

Under visible light irradiation, electrons are excited from the valence band to the conduction band, forming electron-hole pairs. Electrons react with O_2 to generate $\bullet O_2^-$. Cu nanoparticles act as electron traps to promote charge separation. $\bullet O_2^-$ can further transform into $^1O_2$ and $\bullet OH$. These active species work together to degrade TCH into CO_2 and H_2O.

4 Conclusions

In this work, a series of Cu-loaded CeO_2 photocatalysts were successfully synthesized via a hydrothermal method and used for visible-light-driven degradation of tetracycline hydrochloride. Cu loading effectively regulates the band structure, light absorption, and charge transfer behavior of CeO_2. The 15 wt% Cu-CeO_2 composite exhibits the optimal performance with 85.3% TCH degradation efficiency within 60 min, and the rate constant is 5.12 times higher than that of pure CeO_2.

The enhanced photocatalytic performance is mainly ascribed to the extended visible-light response, reduced bandgap, and efficient separation of photogenerated carriers induced by Cu nanoparticles. In addition, the catalyst shows good stability and reusability in cycling tests. This work proves that low-cost Cu can serve as a high-efficiency cocatalyst for CeO_2, and the Cu-CeO_2 composite possesses great potential in the treatment of antibiotic-containing wastewater.

Cu-Loaded CeO_2 Photocatalysts for Visible-Light Degradation of Tetracycline Hydrochloride

Abstract

In this work, a number of Cu nanoparticle-supported CeO_2 (Cu-CeO_2) photocatalysts were successfully synthesized through a hydrothermal approach, and their performance for tetracycline hydrochloride (TCH) removal was evaluated. Experimental results revealed that 15 wt% Cu-CeO_2 presented the highest photocatalytic activity, which decomposed 85.3% of TCH within 60 min under visible-light illumination. The apparent reaction rate constant was measured as 33.84×10^{-3} min^{-1}, 5.12 times greater than that of pure CeO_2. The improved photocatalytic behavior is closely associated with the reduced bandgap, expanded optical absorption range, and promoted charge carrier separation efficiency induced by Cu loading. According to characterization results and quenching tests, a feasible photocatalytic mechanism for TCH degradation in the Cu-CeO_2 system was proposed.

Keywords: CeO_2; Cu loading; tetracycline hydrochloride; photocatalyst

1 Introduction

Cerium oxide has become one of the most widely studied semiconductor photocatalysts owing to its low toxicity, low cost, and excellent chemical stability. Nevertheless, the practical application of pure CeO_2 is largely restricted by its wide bandgap and the rapid recombination of photoexcited charge carriers. Loading noble metal cocatalysts has been widely recognized as an effective modification route. For instance, Keshvadi et al. deposited Ag nanoparticles onto CeO_2 via a wet impregnation strategy. The Ag-CeO_2 composite exhibited enhanced photocatalytic degradation activity toward methylene blue, which was attributed to the improved separation efficiency of photogenerated carriers and the broadened spectral response range. Huang et al. prepared Au-modified CeO_2 nanorods by a hydrothermal method, which showed outstanding photocatalytic degradation efficiency toward tetracycline under visible-light irradiation.

The boosted performance was mainly ascribed to the enhanced visible-light absorption, narrowed bandgap, and improved separation efficiency of electron-hole pairs induced by Au deposition. However, the high cost and limited reserves of noble metals hinder their large-scale practical application. Therefore, it is particularly critical to develop low-cost, high-performance CeO_2-based photocatalysts without noble metals for wastewater treatment. According to previous studies, copper is considered to be a low-cost, non-toxic, and efficient cocatalyst candidate. For example, our group previously synthesized Cu-modified Bi_2O_2S nanoflowers via a hydrothermal route.

The improved electron transport efficiency and narrowed bandgap of Cu-Bi_2O_2S contributed to a higher TCH degradation efficiency. Cu-Bi_2O_2 removed 93.5% of TCH within 60 min under

visible-light irradiation, which was remarkably superior to pure Bi_2O_2S. Therefore, it is feasible to adopt Cu as a cocatalyst to modify CeO_2 so as to achieve efficient photocatalytic elimination of antibiotics. In this study, Cu-loaded CeO_2 (Cu-CeO_2) photocatalysts were fabricated via a facile hydrothermal method. Benefiting from the enhanced electron-hole separation efficiency and improved light harvesting capability, the optimized Cu-CeO_2 sample exhibited significantly enhanced photocatalytic TCH removal performance compared with bare CeO_2. Finally, combined with quenching experiments, a possible photocatalytic degradation mechanism was proposed.

2 Experimental

2.1 Synthesis of Cu-Loaded CeO_2 Hybrid Photocatalyst

Pure CeO_2 was prepared via a hydrothermal method according to earlier reports. The synthetic procedure of Cu-CeO_2 photocatalysts is schematically illustrated in Fig. 1a. In a typical synthesis, 100 mg of as-prepared CeO_2 and a certain amount of $CuSO_4 \cdot 5H_2O$ were dissolved in 10 mL deionized water and stirred for 30 min. Then, 600 μL of 1 M NaOH solution was introduced, and the mixture was stirred continuously for another 30 min. Subsequently, 500 μL of 1 M $NaBH_4$ solution was added dropwise, followed by stirring for 1 h. The precipitate was collected, washed with deionized water, and dried at 60 °C overnight to obtain 5 wt%, 15 wt%, and 20 wt% Cu-CeO_2 samples by adjusting the precursor dosage.

2.3 Characterization

X-ray diffraction (XRD) patterns were recorded on a Rigaku Miniflex 600 diffractometer to identify crystal phase structures. Surface elemental compositions and chemical valence states were determined by X-ray photoelectron spectroscopy (XPS) on a Thermo Fisher Scientific ESCALab 250Xi spectrometer. Microstructural features and elemental distribution were observed using scanning electron microscopy (SEM, ZEISS Crossbeam 540). In addition, UV-Vis diffuse reflectance spectra (DRS) were obtained using an Agilent Cary 100 UV-Vis spectrophotometer.

2.4 Photocatalytic Degradation of TCH

In a typical test, 20 mg of photocatalyst was uniformly dispersed in 40 mL of 50 mg/L TCH solution. The suspension was magnetically stirred in darkness for 30 min to establish adsorption-desorption equilibrium. A 150 W Xe lamp was used as the visible-light source. During light irradiation, 3.5 mL of the reaction solution was taken out every 10 min and filtered to remove catalyst particles. The absorbance of the supernatant was measured at the characteristic absorption peak of 375 nm using a UV-Vis spectrophotometer (Agilent Cary 100). All experiments were conducted in duplicate, and average values were used for plotting.

3 Results and Discussion

Fig. 1b presents the XRD patterns of CeO_2 and Cu-CeO_2 samples. The diffraction peaks located at 28.5°, 33.1°, 47.5°, 56.3°, and 59.1° correspond to the (111), (200), (220), (311), and (222) crystal planes of cubic fluorite-structured CeO_2 (PDF#34-0394), respectively. No characteristic diffraction peaks of Cu (PDF#04-0836) are observed in the 5 wt% Cu-CeO_2 sample, which is attributed to the high dispersion of Cu nanoparticles on the CeO_2 surface. With increasing Cu loading, characteristic diffraction peaks corresponding to the (111), (200), and (220) crystal planes of Cu appear at 43.3°, 50.4°, and 74.1°, respectively.

Fig. 1c displays the UV-Vis absorption spectra of pure CeO_2 and 15 wt% Cu-CeO_2. Clearly, 15 wt% Cu-CeO_2 shows significantly enhanced absorption intensity in the visible-light region, which arises from the surface plasmon resonance effect induced by Cu nanoparticles. The bandgap values of different samples were calculated using the Tauc method. The bandgap of pure CeO_2 is 3.10 eV, while that of 15 wt% Cu-CeO_2 decreases to 2.74 eV, indicating stronger visible-light utilization and higher photocatalytic reactivity.

Fig. 1d and 1e show the SEM images of CeO_2 and Cu-CeO_2, respectively. The samples exhibit a nanorod morphology with a length of approximately 200 nm, and Cu nanoparticles are uniformly distributed on the surface of CeO_2. After Cu loading, the overall morphology of the sample remains unchanged, indicating that the introduction of Cu nanoparticles does not damage the original structure of CeO_2. In addition, EDX elemental mapping images (Fig. 1f-i) confirm that Cu, Ce, and O elements are homogeneously distributed in the Cu-CeO_2 composite.

Fig. 2a shows the XPS survey spectra of CeO_2 and 15 wt% Cu-CeO_2. Compared with pure CeO_2, the Cu-CeO_2 sample presents additional characteristic peaks of Cu 2p, confirming that Cu species have been successfully introduced onto the CeO_2 surface. Fig. 2b shows the Ce 3d XPS spectra of the samples. Peaks located at 884.41, 887.89, 891.01, and 900.36 eV belong to Ce $3d_5/_2$, while peaks at 903.28, 906.39, 909.64, and 918.52 eV are assigned to Ce $3d_3/_2$. Among them, peaks at 887.89 and 906.39 eV correspond to Ce^{3+} species, and the other peaks are attributed to Ce^{4+}.

Compared with pure CeO_2, the relative intensity of the Ce^{3+} characteristic peak in 15 wt% Cu-CeO_2 increases significantly, which is due to the fact that Cu nanoparticles promote the transformation from Ce^{4+} to Ce^{3+}. High-resolution O 1s XPS spectra of pure CeO_2 and Cu-CeO_2 are shown in Fig. 2c. Peaks at 529.45 and 529.68 eV correspond to lattice oxygen, while peaks at 531.74 and 531.81 eV are ascribed to adsorbed oxygen. The Cu 2p XPS spectrum (Fig. 2d) shows that peaks at 933.74 and 953.38 eV correspond to Cu^0 $2p_3/_2$ and $2p_1/_2$, respectively, while peaks at 934.76 and 955.06 eV belong to Cu^{2+} $2p_3/_2$ and $2p_1/_2$.

Satellite peaks located at 941.97, 944.56, and 962.93 eV further verify the existence of Cu^{2+}, which may be caused by the partial oxidation of Cu nanoparticles during the preparation process.

Fig. 3a shows the photocatalytic degradation efficiency of TCH and the corresponding reaction kinetic constants over different samples. After 60 min of visible-light irradiation, the degradation efficiency of pure CeO_2 is only 34.1%. The photocatalytic activity is significantly improved after Cu loading. Among all samples, 15 wt% Cu-CeO_2 shows the optimal degradation performance, with a degradation efficiency of 85.3% and a maximum reaction rate constant of 33.84×10^{-3} min^{-1}.

When the Cu content is further increased to 20 wt%, the degradation efficiency decreases to 66.8%, which is attributed to the aggregation of excess Cu nanoparticles on the catalyst surface that occupy active sites. As shown in Fig. 3c, at pH 3.0 and pH 9.0, the degradation efficiencies of 15 wt% Cu-CeO_2 are only 17.2% and 34.2%, respectively. This phenomenon can be explained as follows: (1) in an acidic environment, H^+ occupies active sites and hinders TCH adsorption; (2) in an alkaline environment, OH^- reacts with Cu^{2+} to form $Cu(OH)_2$ and CuO, thus suppressing the photocatalytic reaction.

Fig. 3d and 3e illustrate the effects of different inorganic anions and cations on the photocatalytic activity of 15 wt% Cu-CeO_2. Notably, the degradation efficiency of TCH decreases to 32.6% in the presence of SO_4^{2-}, which is attributed to the quenching effect of SO_4^{2-} on $\cdot O_2^-$ radicals. In addition, Ca^{2+} and Mn^{2+} also exert strong inhibitory effects on TCH degradation, which is likely due to the high charge density of Ca^{2+} and Mn^{2+} leading to competitive adsorption on the Cu-CeO_2 surface and blocking active sites. As shown in Fig. 3f, the degradation efficiency of 15 wt% Cu-CeO_2 remains above 76% after three consecutive cycles, indicating good cycling stability.

Fig. 4a presents the valence band XPS spectra of CeO_2 and 15 wt% Cu-CeO_2. The valence band positions are determined to be 1.32 eV and 0.23 eV, respectively. Based on the bandgap values (3.10 eV for CeO_2 and 2.74 eV for 15 wt% Cu-CeO_2), the conduction band positions are calculated to be −1.78 eV and −2.51 eV, respectively. Fig. 4b shows the PL spectra of CeO_2 and Cu-CeO_2 under 370 nm excitation. The PL intensity of Cu-CeO_2 is lower than that of pure CeO_2, indicating that Cu loading effectively suppresses the recombination of photogenerated electron-hole pairs and improves the photocatalytic degradation activity of TCH.

Fig. 4c shows the results of quenching experiments. EtOH, IPA, BQ, and FA were used as scavengers for h^+, $\cdot OH$, $\cdot O_2^-$, and $^1O_2$, respectively. After adding these scavengers, the TCH degradation efficiency decreases from 85.3% to 76.5%, 52.9%, 31.2%, and 56.4%, respectively, indicating that $\cdot O_2^-$ is the primary reactive species in the degradation process.

Based on the above results, the photocatalytic degradation process over the Cu-CeO_2 composite can be described as follows (Fig. 4d): Under light irradiation, electrons in the VB of Cu-CeO_2 are excited into the CB, generating e^--h^+ pairs. The electrons in the CB of Cu-CeO_2 possess stronger reducibility than O_2/ $\cdot O_2^-$ (−0.33 eV vs NHE), thus promoting the formation of $\cdot O_2^-$. Meanwhile, some electrons are captured by Cu nanoparticles and migrate to the catalyst surface, enabling

rapid separation of e^--h^+ pairs.

Part of $\cdot O_2^-$ undergoes energy transfer at the interface to produce $^1O_2$, while another part undergoes disproportionation to form H_2O_2. The generated H_2O_2 can be further reduced by CB electrons to produce $\cdot$OH. Therefore, $\cdot O_2^-$, $^1O_2$, and $\cdot$OH act synergistically to participate in the degradation of TCH.

4 Conclusions

In summary, a series of Cu-loaded CeO_2 photocatalysts were successfully prepared via a hydrothermal method and applied for the visible-light-driven degradation of tetracycline hydrochloride. The 15 wt% Cu-CeO_2 composite exhibits outstanding photocatalytic performance, and its reaction rate constant is 5.12 times higher than that of pure CeO_2. The enhanced activity is mainly attributed to the expanded visible-light absorption, narrowed bandgap, and promoted separation of photogenerated charge carriers induced by Cu loading.

This study confirms that low-cost and environmentally friendly Cu nanoparticles can serve as high-efficiency cocatalysts for constructing high-performance CeO_2-based photocatalysts, which exhibit promising application potential in the purification of antibiotic-contaminated wastewater.

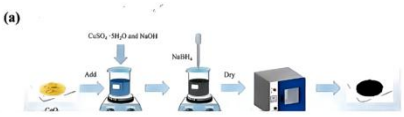
(a)
CuSO4 ·5H2O and NaOH
Add
NaBH4
Dry

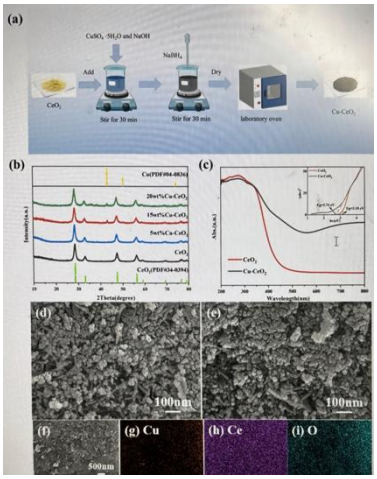
(a)
CuSO4 ·5H2O and NaOH
Add
NaBH4
Dry
Stir for 30 min
Stir for 30 min
laboratory oven
(b)
(c)
(d)
(e)
100nm
100nm
(f)
500nm
(g) Cu
(h) Ce
(i) O

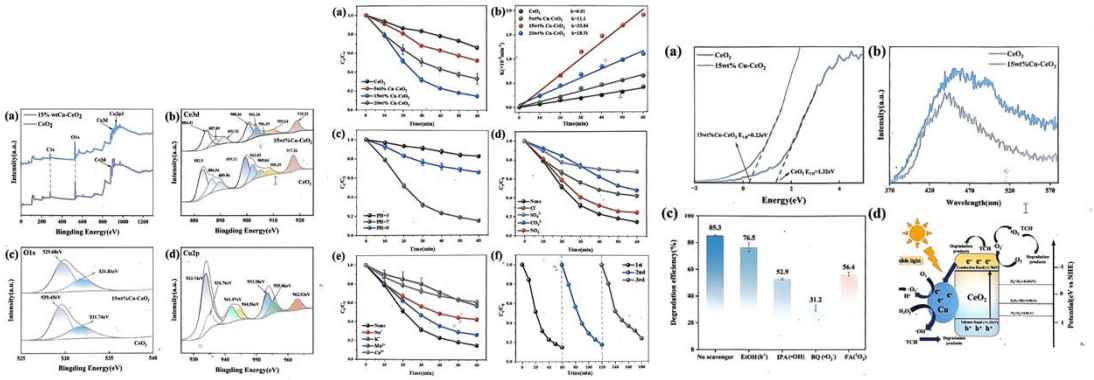
(a)
(b)
(c)
(d)
(e)
(f)
Binding Energy(eV)
Time(min)
Energy(eV)
Wavelength(nm)
Degradation efficiency(%)
85.3
76.5
52.9
31.2
56.4
No scavenger
EtOH(h+)
IPA(•OH)
BQ(•O2-)
FA(1O2)
Potential(eV vs NHE)

References

[1] Ma J, Chen Y, Zhou G, et al. Recent advances in photocatalytic degradation of tetracycline antibiotics[J]. Catalysts, 2024, 14(11): 762.

[2] Yu H, Zhang X, Zhao J, et al. Mechanism of TiO_2 nanotube UV-photocatalytic degradation of antibiotic resistance genes in the wastewater sludge and blocking of the transfer[J]. Frontiers in Environmental Science, 2025, 13: 1590101.

[3] Liu J, Ruan H, Duan P, et al. Photocatalytic Degradation of Antibiotics Using Nanomaterials: Mechanisms, Applications, and Future Perspectives[J]. Nanomaterials, 2025, 16(1): 49.

[4] Aziz K H H, Mustafa F S, Karim M A H, et al. Pharmaceutical pollution in the aquatic environment: advanced oxidation processes as efficient treatment approaches: a review[J]. Materials Advances, 2025, 6(11): 3433-3454.

[5] Subasi B, Hayri-Senel T, Kahraman E, et al. Photocatalytic degradation of tetracycline from aqueous solution with graphene oxide and hydroxyapatite composites[J]. Scientific Reports, 2025, 15(1): 25894.

[6] Yao J, Dong Z, Ye X, et al. Electrochemically activated peroxymonosulfate with mixed metal oxide electrodes for sulfadiazine degradation: Mechanism, DFT study and toxicity evaluation[J]. Chemosphere, 2022, 309: 136695.

[7] Han Z K, Liu W, Gao Y. Advancing the understanding of oxygen vacancies in ceria: Insights into their formation, behavior, and catalytic roles[J]. JACS Au, 2025, 5(4): 1549-1569.

[8] Lin H, Han X, Tang Y, et al. Tannic acid-mediated oxygen vacancies in broccoli-like CeO_2 @Carbon for enhanced photocatalytic peroxymonosulfate activation toward Tetracycline degradation[J]. Environmental Research, 2025: 123268.

[9] Dhanka A K, Pani B, Agasti N. Defect-enriched CuO/CeO_2 nanostructure: in-depth structural characterization and photocatalytic performance[J]. RSC Advances, 2025, 15(15): 11774-11779.

[10] Alrahili M R, Rafea M A, Zaki M E A, et al. Rationally designed Inr-CeO_2/g-C_3N_4 S-scheme heterojunction photocatalyst with tuned redox ability for the photocatalytic degradation of pharmaceutical contaminants[J]. RSC Advances, 2025, 15(55): 47271-47281.

[11] Deng S, Wang H, Dong Y, et al. Morphology effect on the photocatalytic performance of CeO_2 and insights into the degradation mechanism of tetracycline[J]. Journal of Environmental Chemical Engineering, 2025, 13(1): 115216.

[12] Zhang H, Luo W, Sun H, et al. Ce-doped nanosheet as visible light photocatalyst for the photocatalytic degradation of tetracycline hydrochloride[J]. ACS Applied Nano Materials, 2024, 7(10): 11506-11517.

[13] Habib N R, Taddesse A M, Sainz R, et al. Copper-loaded sustainable MOFs as photocatalysts for dye removal[J]. Journal of Photochemistry and Photobiology A: Chemistry, 2024, 456: 115842.

[14] Liu S, Chen X, Yu J, et al. Interfacial synergy between Cu nanoclusters and oxygen vacancies on CeO_2 for enhanced selective photoreduction of CO_2 to C_2H_4[J]. Journal of Materials Chemistry A, 2025, 13(36): 30095-30107.

[15] Panda J, Priyadarshini N, Mansingh S, et al. Ce/Cu-MOF-Derived AgAu-C/N-CeO_2@C/N-CuO S-Scheme Nanohybrids for Photocatalytic H_2O_2 Production and Photo-Fenton Antibiotic Degradation[J]. Langmuir, 2025, 41(46): 31456-31470.

[16] Shang Z, Yu Y, Yang H, et al. One-step solution combustion synthesis of micro-nano-scale porous Cu/CeO_2 with enhanced photocatalytic properties[J]. Journal of Rare Earths, 2023, 41(2): 250-258.

[17] Mohamed M V, Ahamed A J, Begum A S, et al. Investigation of the anticancer, antibacterial, and photocatalytic properties of CeO_2 and Cu-CeO_2 nanoparticles synthesized by a green method[J]. Green Chemistry Letters and Reviews, 2025, 18(1): 2543911.

[18] Jia X, Wang F, Xu X, et al. Highly efficient photocatalytic degradation of tetracycline by modifying UiO-66 via different regulation strategies[J]. ACS Omega, 2023, 8(30): 27375-27385.

[19] Hu M, Chen W, Wang J. Photocatalytic degradation of tetracycline by La-Fe Co-doped $SrTiO_3$ /TiO_2 composites: performance and mechanism study[J]. Water, 2024, 16(2): 210.

[20] Zhao Y, Xu Y, Yu C, et al. Surface interface modulation and photocatalytic membrane technology for degradation of oily wastewater[J]. Catalysts, 2025, 15(8): 730.

[21] 刘文琦. 不同形貌二氧化铈的合成及其复合光催化剂的性能研究[D]. 北京化工大学, 2021.

[22] Nejat Redwan Habib, Abi M. Taddesse, Raquel Sainz, Manuel Sanchez-Sanchez, Isabel Diaz, Copper-loaded sustainable MOFs as photocatalysts for dye removal, Journal of Photochemistry and Photobiology A: Chemistry, 2024, 456: 115842.

[23] Yang P, Zhou S, Lei J. Preparation of Ordered Mesoporous Nanocrystalline Ceria and Ceria-Zirconia for Soot Oxidation[J]. Journal of Wuhan University of Technology-Mater. Sci. Ed., 2016, 31: 113-117.

[24] On the analysis of diffuse reflectance measurements to estimate the optical properties of amorphous porous carbons and semiconductor/carbon catalysts.

[25] One-step solution combustion synthesis of micro-nano-scale porous Cu/CeO_2 with enhanced photocatalytic properties.

[26] One-step solution combustion synthesis of micro-nano-scale porous Cu/CeO_2 with

enhanced photocatalytic properties.

[27] Gu Y, Cai T, Gao X, et al. Catalytic Combustion of Chlorinated Aromatics over WOx/CeO_2 Catalysts at Low Temperature[J]. Applied Catalysis B: Environmental, 2019, 248: 264-276.

[28] G J, Zhang X, Zhang A, et al. CeO_2-CuO/Cu_2O/Cu Monolithic Catalysts with Three-Kind Morphologies Cu_2O Layers for Preferential CO Oxidation[J]. Applied Surface Science, 2018, 434: 44-51.

[29] Lykaki M, Pachatouridou E, Iliopoulou E, Carabineiro S A C, Konsolakis M. Impact of the synthesis parameters on the solid state properties and the CO oxidation performance of ceria nanoparticles[J]. RSC Advances, 2017, 7(10): 6160.

[30] Ce 3d XPS investigation of cerium oxides and mixed cerium oxide (CexTiyOz).

[31] Catalytic Properties of Ceria and CeO_2-Containing Materials Binding energy referencing in X-ray photoelectron spectroscopy.

[32] Luo Y, Estudillo-Wong L A, Cavillo L, et al. An easy and cheap chemical route using a MOF precursor to prepare Pd-Cu electrocatalyst for efficient energy conversion cathodes[J]. Journal of Catalysis, 2016, 338: 135-142.

[33] Huang J, Zheng H, Xu H, et al. Magnetic bimetallic Fe and Cu-loaded N-doped biochar for the activation of peroxomonosulfate for tetracycline degradation: DFT calculations and mechanism analysis[J]. Applied Surface Science, 2025, 679: 161158.

[34] Xi Y, Xiao Z, Lv H, et al. Construction of CuO/Cu-nanoflowers loaded on chitosan-derived porous carbon for high energy density supercapacitors[J]. Journal of Colloid and Interface Science, 2023, 630: 52-54.

[35] Li Z, Liu J, Gao B, et al. Cu-Mn-CeOx loaded ceramic catalyst for non-thermal sterilization and microwave thermal catalysis of VOCs degradation[J]. Chemical Engineering Journal, 2022, 442: 136288.

[36] Binding energy referencing in X-ray photoelectron spectroscopy.

[37] Nejat Redwan Habib, Abi M. Taddesse, Raquel Sainz, Manuel Sanchez-Sanchez, Isabel Diaz, Copper-loaded sustainable MOFs as photocatalysts for dye removal[J]. Journal of Photochemistry and Photobiology A: Chemistry, 2024, 456: 115842.

[38] Photocatalytic degradation of a mixture of eight antibiotics using Cu-modified TiO_2 photocatalysts: Kinetics, mineralization, antimicrobial activity elimination and disinfection.

[39] Enhancing photocatalytic hydrogen production: The impact of copper loading on Cu-doped TiNT and CuO/TiNT heterostructures.

[40] Enhanced visible-light-driven photocatalytic degradation of tetracycline wastewater using surfactant-modified Au-loaded CeO_2 nanorods.

[41] Kosmulski M. The pH dependent surface charging and points of zero charge. IX. Update[J]. Advances in Colloid and Interface Science, 2021, 296: 102519.

[42] Padré C T, Keating P R L, Riter R E, et al. pH-Dependent Spectroscopy of Tetracycline and Its Analogs[J]. Journal of Fluorescence, 2014, 24: 1183-1198.

[43] Mojica E R E, Nguyen E, Rozov M, Bright F V. pH-Dependent Spectroscopy of Tetracycline and Its Analogs[J]. Journal of Fluorescence, 2014, 24: 1183-1198.

[44] Zhang Y, et al. A review of copper-based Fenton reactions for the removal of organic pollutants from wastewater over the last decade: different reaction systems[J]. Environmental Science and Pollution Research, 2024, 31: 27609-27633.

[45] Toth T, Czaplicka M, et al. Rate constants of dichloride radical anion reactions with molecules of environmental interest: a review[J]. Environmental Science and Pollution Research, 2021.

[46] Liou S Y, Dodd M C. Evaluation of hydroxyl radical and reactive chlorine species generation from the superoxide/hypochlorous acid reaction as the basis for a novel advanced oxidation process[J]. Water Research, 2021, 200: 117142.

[47] Performance of Copper as a Catalyst for Fenton-like Processes in Highly Saline Solutions, 2025.

[48] Wang X, Li M, Wu Z. In situ spectroscopic insights into the redox and acid-base properties of ceria catalysts[J]. Chinese Journal of Catalysis, 2021.

[49] Zhang Q, et al. Effect of inorganic anions on the performance of advanced oxidation processes for degradation of organic contaminants[J]. Chemical Engineering Journal, 2021, 406: 126877.

[50] Yan M, et al. Carbonate radicals in environmental systems: mechanistic insights and engineering applications[J]. Water Research, 2025.

[51] Zhou W, et al. The impact of chloride and nitrogenous ions on advanced oxidation processes: Radical formation, pollutant removal, transformation products, and toxicity changes[J]. Environmental Functional Materials, 2025.

[52] Chen H, et al. Adsorption Characteristics of Tetracycline onto Biochars as Affected by Solution Chemistry Conditions and Ball Milling Treatment[J]. Water, Air, & Soil Pollution, 2020, 231: 441.

[53] Daghrir R, Drogui P. Tetracyclines metal complexation: Significance and fate of mutual existence in the environment[J]. Environmental Pollution, 2017, 221: 1-14.

[54] Activity, selectivity, and stability of earth-abundant CuO/Cu_2O/Cu-based photocatalysts toward CO_2 reduction.

[55] Effects of the Crystalline Properties of Hollow Ceria Nanostructures on a CuO-CeO_2 Catalyst in CO Oxidation.

[56] Recent progress of modified CeO_2-based materials for photocatalytic environmental remediation and antibacterial activity.

[57] Nanostructured CeO_2 photocatalysts: optimizing surface chemistry and morphology[J]. Nanoscale, 2024.

[58] Construction of Cu^{2+}-doped CeO_2 nanocrystals hierarchical hollow spheres[J]. Journal of Materials Science: Materials in Electronics, 2021.

[59] A comprehensive review of oxygen vacancy modified photocatalysts[J]. Physical Chemistry Chemical Physics, 2024.

[60] Photocatalytic activity of metal oxides-The role of holes and OH radicals[J]. Applied Catalysis B: Environmental, 2011.

[61] Oxygen-vacancy engineering and junction design in CeO_2 nanomaterials for photocatalytic pollutant degradation, 2025.